

BIOCHEMISTRY

Real-time single-molecule observation of chaperone-assisted protein folding

Nicholas R. Marzano^{1,2}, Bishnu P. Paudel^{1,2}, Antoine M. van Oijen^{1,2*†‡}, Heath Ecroyd^{1,2*†‡}

The ability of heat shock protein 70 (Hsp70) molecular chaperones to remodel the conformation of their clients is central to their biological function; however, questions remain regarding the precise molecular mechanisms by which Hsp70 machinery interacts with the client and how this contributes toward efficient protein folding. Here, we used total internal reflection fluorescence (TIRF) microscopy and single-molecule fluorescence resonance energy transfer (smFRET) to temporally observe the conformational changes that occur to individual firefly luciferase proteins as they are folded by the bacterial Hsp70 system. We observed multiple cycles of chaperone binding and release to an individual client during refolding and determined that high rates of chaperone cycling improves refolding yield. Furthermore, we demonstrate that DnaJ remodels misfolded proteins via a conformational selection mechanism, whereas DnaK resolves misfolded states via mechanical unfolding. This study illustrates that the temporal observation of chaperone-assisted folding enables the elucidation of key mechanistic details inaccessible using other approaches.

INTRODUCTION

Most proteins fold into specific three-dimensional conformations to carry out their unique biological roles (1). However, during periods of cellular stress or in response to genetic mutation, proteins can become misfolded. This process can contribute to the progression of diseases associated with protein loss of function (e.g., cystic fibrosis) (2) or the accumulation of protein aggregates, as occurs in Parkinson's disease, Alzheimer's disease, and cataracts (3–5). Consequently, cells have evolved a complex network of molecular chaperones that act to prevent protein misfolding and maintain protein homeostasis (6–8). The Hsp70 family of molecular chaperones represents a central hub of this network, performing a plethora of cellular roles including de novo protein folding and refolding, protein disaggregation, protein translocation, and the assembly and disassembly of protein complexes (9, 10). The mechanisms by which Hsp70 folds client proteins are highly regulated by its co-chaperones Hsp40 and nucleotide exchange factors (NEFs).

Much of our current understanding regarding the mechanisms by which Hsp70 folds its client proteins has been elucidated through the bacterial system that comprises a single Hsp70 (DnaK), Hsp40 (DnaJ), and NEF (GrpE) (11–14). The current consensus of Hsp70 function is that protein folding is initiated upon binding of a misfolded or unfolded client by Hsp40, which delivers the client to the adenosine 5'-triphosphate (ATP)-bound Hsp70. Binding of the Hsp40-client complex to Hsp70 stimulates the rate of hydrolysis of ATP to adenosine 5'-diphosphate (ADP) by more than 1000-fold (15, 16), which results in high-affinity capture of the bound client by Hsp70. Binding of a NEF to ADP-bound Hsp70 accelerates the release of ADP, which results in concomitant rebinding of ATP and returns Hsp70 to the low-affinity "open conformation."

Consequently, the client protein dissociates from Hsp70 and can either spontaneously refold to the native state or become misfolded and be subjected to additional rounds of chaperone binding and release.

Because of the heterogeneous nature of chaperone-client interactions and the conformational state of the client, fundamental questions remain regarding the precise molecular mechanisms by which chaperones remodel the conformation of their clients. For instance, it is unclear whether chaperones stabilize unfolded conformers within a misfolded ensemble (e.g., conformational selection) (17) or whether they use ATP hydrolysis to mechanically unfold client proteins (in the case of Hsp70) (18–21). Furthermore, it remains to be determined whether chaperones promote protein folding by introducing structural and entropic constraints on the polypeptide that minimize non-native interactions or smooth folding landscapes. These mechanistic insights are crucial in our understanding of how chaperones work to fold proteins but are typically difficult to elucidate using conventional ensemble-averaging approaches. This limitation is largely because the rare and transient states that are inherently present during chaperone-assisted folding are masked by billions of asynchronous molecules visiting those states at different times.

Single-molecule approaches have become increasingly popular as a tool to better understand the fundamental mechanisms of chaperone function owing to their capacity to directly observe single molecules and detect kinetic features and states that are normally hidden. Consequently, these approaches have been applied to study how molecular chaperones affect the conformational state of their client proteins and assist in their refolding (18, 19, 22). However, while these previous studies have provided valuable insights, most of them did not allow for long-term visualization of the folded state of the same molecule.

In this work, we have directly observed the conformational changes that occur to individual client proteins as they are folded by the bacterial Hsp70 system [e.g., DnaK, DnaJ, and GrpE (denoted as KJE)] with temporal resolution. To do so, we developed a firefly luciferase (Fluc) construct that can be immobilized to a

Copyright © 2022
The Authors, some
rights reserved;
exclusive licensee
American Association
for the Advancement
of Science. No claim to
original U.S. Government
Works. Distributed
under a Creative
Commons Attribution
NonCommercial
License 4.0 (CC BY-NC).

¹Molecular Horizons and School of Chemistry and Molecular Bioscience, University of Wollongong, Wollongong, New South Wales 2522, Australia. ²Illawarra Health and Medical Research Institute, Wollongong, New South Wales 2522, Australia.

*Corresponding author. Email: heathe@uow.edu.au (H.E.); vanoijen@uow.edu.au (A.M.v.O.)

†Lead contacts.

‡These authors contributed equally to this work.

coverslip surface such that the conformation of individual Fluc molecules can be monitored over time using total internal reflection fluorescence (TIRF) microscopy and single-molecule fluorescence resonance energy transfer (smFRET). By analyzing the kinetic data generated from FRET trajectories of individual molecules, we demonstrate that DnaJ remodels misfolded proteins via a conformational selection mechanism, whereas DnaK conformationally expands the client via mechanical unfolding. We provide direct evidence that Fluc undergoes repeated cycles of chaperone binding and release during refolding and that the rate of chaperone cycling correlates with an improved refolding yield.

RESULTS AND DISCUSSION

The conformation of Fluc^{IDS} can be monitored in real time using smFRET and TIRF microscopy

Fluc was chosen for this work as it has several characteristics that make it an ideal client protein for the study of chaperone function; Fluc readily misfolds following dilution from chemical denaturant and has a limited ability to spontaneously fold or refold (it requires chaperones to do so), and the attainment of its native state can be readily assessed via a highly sensitive bioluminescence enzymatic assay (23–25). To use Fluc as a sensor of protein folding using smFRET, we used a Fluc construct in which all native cysteines were substituted with alanines and two cysteine residues were introduced for fluorescent labeling with a donor and acceptor fluorophore pair. The introduced cysteines are positioned on the external faces of the N-terminal domain (K141C) and C-terminal domain (K491C) of Fluc and span either side of the interdomain cleft (Fig. 1A). The modified Fluc construct (i.e., Fluc^{ΔCys, K141C, K491C}) is here denoted as Fluc^{IDS}, because the introduced cysteines enable the relative structure and positioning of both Fluc domains to be monitored via smFRET and, thus, act as an interdomain sensor of protein folding.

We first characterized the ability of Fluc^{IDS} to report on conformational changes in real time (Fig. 1A). To do so, we immobilized Fluc^{IDS} to a neutravidin-functionalized coverslip and imaged it in the presence of different concentrations of denaturant using TIRF microscopy and microfluidics (Fig. 1B). Native Fluc^{IDS} resulted in an FRET distribution centered at ~0.7 (Fig. 1C), with most molecules exhibiting consistent FRET values or, less commonly, dynamic changes in FRET efficiency over time (fig. S1A). We observed that the FRET efficiency decreased with increasing concentrations of denaturant such that, when in 4 M guanidinium hydrochloride (GdHCl), the FRET distribution was centered at 0.1. Such a result is consistent with the transition of Fluc^{IDS} to a conformationally expanded random-coil structure that has been observed previously in other single-molecule unfolding experiments (26–29). Progressive dilution of denaturant resulted in an increase in FRET efficiency; however, complete removal of Fluc^{IDS} out of denaturant resulted in Fluc^{IDS} having a FRET efficiency that was higher than that of the native state (~0.9 versus ~0.7, respectively). This high-FRET state corresponds to a previously observed misfolded Fluc conformation, which occurs as a result of the formation of non-native contacts between residues in the N-terminal domain and/or residues in the C-terminal domain (19, 30, 31).

As a proof of principle for the ability of Fluc^{IDS} to act as a real-time sensor of protein folding, immobilized Fluc^{IDS} molecules were alternatively incubated in the absence or presence of chemical

denaturant. FRET intensity originating from individual Fluc^{IDS} species was determined and was collated into an averaged heatmap (Fig. 1, D and E, and fig. S1B). Native Fluc^{IDS} (measured between 0 to 20 s) exhibited a FRET efficiency of ~0.7, which rapidly dropped to ~0.1 for all Fluc^{IDS} molecules measured upon addition of GdHCl. Removal of GdHCl caused the FRET efficiency to rapidly increase to the high-FRET misfolded state (~0.9). Similar transitions to low-FRET and high-FRET states were observed following a second round of injection into and removal of GdHCl from the flow cell. Together, these data highlight that smFRET is an ideal tool to monitor the real-time conformational changes of Fluc^{IDS} and that Fluc^{IDS} can be used as a sensor of protein folding.

Ensemble-based enzymatic assays have established that the bacterial Hsp70 system (i.e., KJE) can efficiently refold chemically denatured Fluc (11–14). Hence, we sought to use this model chaperone system and characterize its ability to refold Fluc^{IDS}, by monitoring the return of luminescence during chaperone-assisted folding, in preparation for smFRET experiments (see Methods). When chemically denatured Fluc^{IDS} was refolded in the absence of chaperones (i.e., spontaneous refolding) or a non-chaperone control protein, ovalbumin, minimal refolding was observed (Fig. 1F). Hence, the high-FRET misfolded species observed previously using smFRET (Fig. 1C) represents an enzymatically inactive state of Fluc^{IDS}. However, Fluc^{IDS} was efficiently refolded by the KJE system, with activity reaching greater than 150% of native (non-denatured) Fluc^{IDS} after 90 min (suggesting that some non-native Fluc^{IDS} was already present in the native sample). Crucially, chaperone-assisted refolding was observed to be efficient only when the NEF, GrpE, was present during the reaction. Data from this work and others (19, 21, 31) have shown that the misfolded (high-FRET) Fluc conformation is stable and enzymatically inactive and persists for many hours. However, the addition of the bacterial Hsp70 system to spontaneously misfolded Fluc^{IDS} resulted in rapid and efficient refolding. Collectively, these results demonstrate that the bacterial Hsp70 system efficiently resolves misfolded states of Fluc^{IDS} and refolds it to a functional state and that GrpE is essential for efficient refolding.

Notably, the amount of spontaneous refolding of Fluc^{IDS} [3.6% of the activity of the native (non-denatured) state] was much lower than previously reported for the spontaneous refolding of wild-type Fluc [Fluc^{WT}; e.g., 58.2% by reference (19)]. To determine whether the low spontaneous refolding yield of Fluc^{IDS} is due to the introduced mutations in this isoform of the protein (i.e., C-terminal AviTag and cysteine substitutions), the refolding experiments were repeated using both Fluc^{IDS} and Fluc^{WT} (fig. S2A). Refolding was performed with lower concentrations of ATP as this slows refolding rates and thus augments differences in the refolding kinetics between these two proteins. Under these conditions, 10-fold more Fluc^{WT} was able to spontaneously refold to the native state (29.6%) compared to Fluc^{IDS} (2.9%). As expected, dilution of Fluc from denaturant in the presence of the bacterial Hsp70 system resulted in the efficient refolding of both Fluc^{WT} and Fluc^{IDS}, although the rate of refolding (determined as the time required to achieve 50% refolding, denoted as $t_{1/2}$) was ~4-fold faster for Fluc^{WT} ($t_{1/2} = 15.9$ min) compared to Fluc^{IDS} ($t_{1/2} = 66.0$ min).

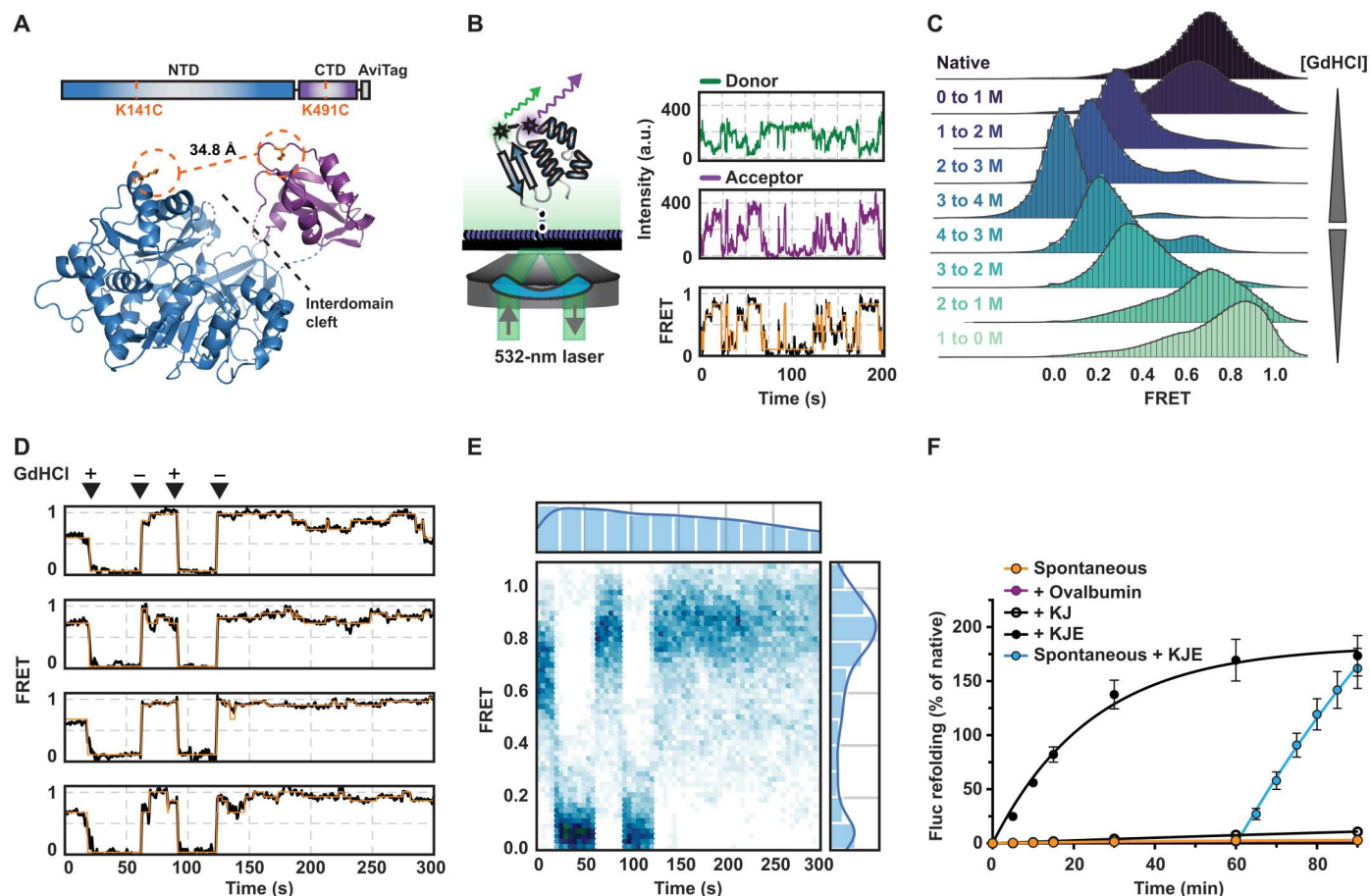


Fig. 1. The conformation of individual Fluc^{IDS} molecules can be monitored in real time using smFRET and can be refolded by the bacterial Hsp70 system. (A) Schematic of the Fluc^{IDS} FRET-construct used in this work (top) and the structure of Fluc^{WT} (Protein Data Bank 1LCI) (60) (bottom). Residues that were mutated to cysteines for labeling with a FRET fluorophore pair and the Ca-Ca distance between labeled residues in the Fluc^{IDS} construct are shown. Fluc^{IDS} contains a C-terminal AviTag motif to enable specific immobilization to a neutravidin-functionalized coverslip surface. NTD, N-terminal domain; CTD, C-terminal domain. (B) Schematic of the smFRET imaging setup. AF555, Alexa Fluor 555 /AF647-labeled Fluc^{IDS} is specifically immobilized to a coverslip surface and is illuminated by a 532-nm laser that selectively excites the AF555 donor fluorophore. The fluorescence from both AF555 and AF647 (acceptor) fluorophores was measured over time, and the FRET efficiency was calculated. a.u., arbitrary units. (C) Ridgeline plot of the FRET efficiency of Fluc^{IDS} molecules when unfolded by increasing concentrations of GdHCl (0 to 4 M) and during refolding following dilution out of denaturant. (D and E) Immobilized Fluc^{IDS} was incubated in imaging buffer supplemented with or without 4 M GdHCl, and the FRET efficiency was measured every 500 ms. Additional traces are shown in fig. S1B. (D) Representative smFRET traces of individual Fluc^{IDS} molecules. The addition (+) and removal (-) of 4 M GdHCl from the flow cell are indicated above the traces. Data are fit with a HMM, Hidden Markov model (shown in orange). (E) The FRET efficiency over time for all Fluc^{IDS} molecules were collated and plotted as a heatmap ($n = 92$ molecules). (F) Fluc^{IDS} (1 μM) in 5 M GdHCl was diluted 100-fold (10 nM final concentration of Fluc^{IDS}) into refolding buffer alone (i.e., spontaneous) or buffer supplemented with molecular chaperones or the non-chaperone control protein, ovalbumin (15 μM). Chaperone-assisted refolding was performed with DnaK (3 μM) and DnaJ (1 μM) only (+KJ) or in combination with GrpE (1.5 μM) (+KJE). Rescue of misfolded Fluc^{IDS} was performed by 10-fold dilution of spontaneously refolded Fluc^{IDS} (1 nM final concentration) into refolding buffer containing DnaK (3 μM), DnaJ (1 μM), and GrpE (1.5 μM) (spontaneous + KJE). All treatments contained 5 mM ATP. Data shown represent the means \pm SEM from three independent experiments.

DnaJ binds to and stabilizes expanded conformations of Fluc^{IDS} via a conformational selection mechanism

We next used smFRET to investigate how DnaJ affects the folded state of Fluc^{IDS} . When Fluc^{IDS} was allowed to refold in the absence of chaperones, it adopted the previously described high-FRET (~ 0.8) misfolded conformation (Fig. 2, A and B). However, when incubated with progressively higher concentrations of DnaJ, the FRET distributions became broader, and a second low-FRET peak centered at ~ 0.2 to 0.3 was observed. The reduced FRET efficiency of Fluc^{IDS} molecules is consistent with the DnaJ-mediated conformational expansion of client proteins observed previously (18).

Kinetically, there are two possible explanations for the increased occupancy of Fluc^{IDS} at low-FRET states when incubated in the presence of DnaJ: (i) Low-FRET states are longer-lived than high-FRET states, or (ii) transitions that result in the accumulation of low-FRET states of Fluc^{IDS} are favored. To interrogate this, individual smFRET trajectories were fit to a Hidden Markov model (HMM) that enables discrete FRET states to be identified and the transition kinetics between these states to be quantitatively analyzed (see Methods). FRET states were classified as high or low (above or below 0.5) and transitions categorized in four different transition classes (high to high, high to low, low to high, and low to low). Using these classifications, the relative occurrence and residence

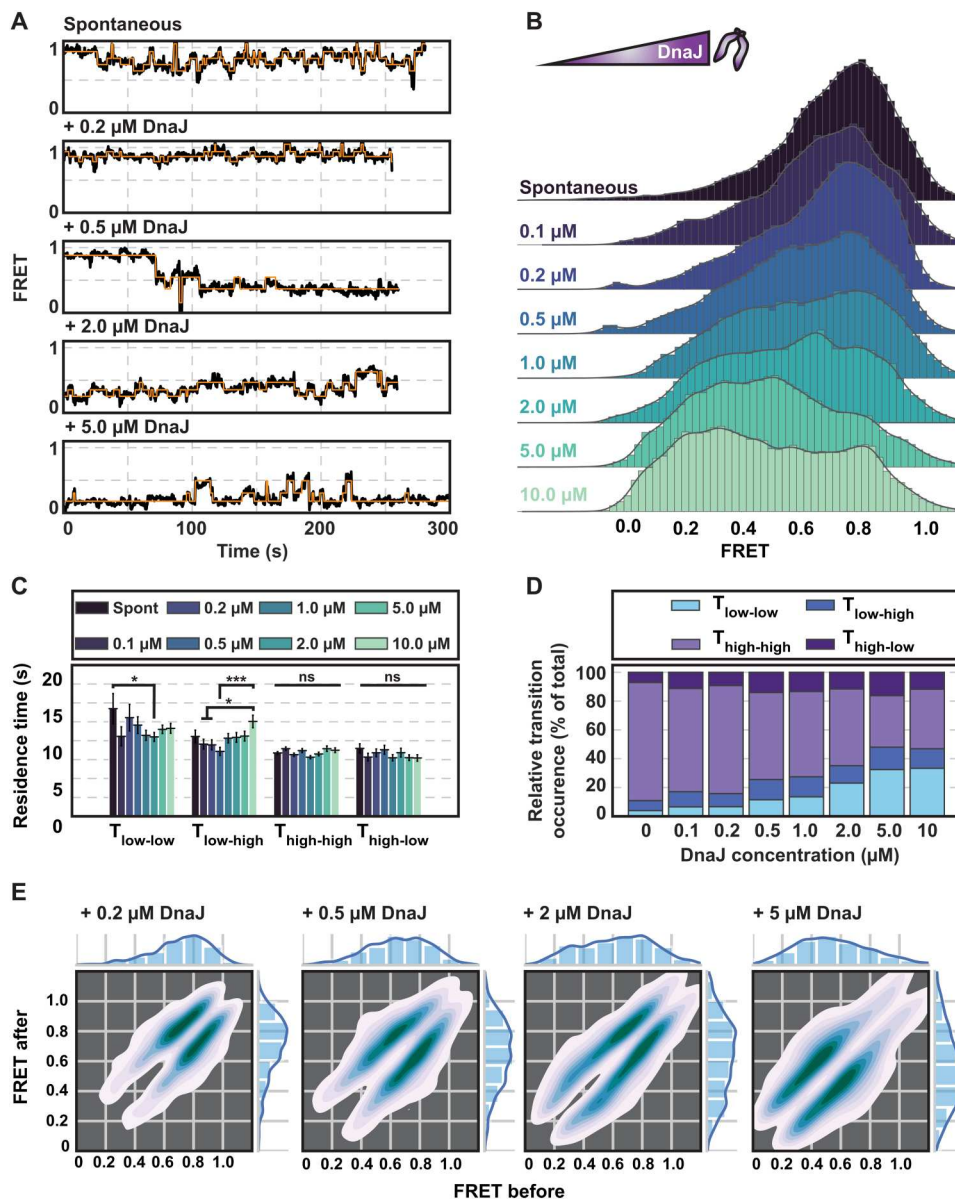


Fig. 2. DnaJ stabilizes conformationally expanded states of Fluc^{IDS}. Fluc^{IDS} was diluted from denaturant in the presence of increasing concentrations of DnaJ (0 to 10 μM), and the FRET efficiency was measured. (A) Representative smFRET traces of individual Fluc^{IDS} molecules when incubated in the absence (i.e., spontaneous) or presence of increasing concentrations of DnaJ (0.2 to 5 μM). Additional traces are shown in fig. S4. (B) Ridgeline plot of the FRET efficiency distributions of misfolded Fluc^{IDS} alone or when incubated with the indicated concentration of DnaJ. (C) Bar plots showing the residence time of different transition classes. Data shown are the means \pm SEM. A two-way analysis of variance (ANOVA) statistical analysis with Tukey's multiple-comparisons post hoc test was performed to determine statistically significant differences in residence times between treatment groups within each transition class. * $P \leq 0.05$ and *** $P \leq 0.001$. ns or the absence of markers indicates no significant difference ($P > 0.05$). (D) Relative transition occurrence of each transition class. (E) TDPs, Transition density plots of Fluc^{IDS} transitions when incubated in the absence or presence of the indicated concentration of DnaJ. Data for all panels were derived and collated from the HMM fits of at least 268 individual Fluc^{IDS} molecules per treatment.

time of each transition class were determined (see fig. S3). Kinetic analysis of individual FRET trajectories demonstrates that the residence times of Fluc^{IDS} molecules are relatively unaffected by increasing concentrations of DnaJ, with the exception that there is an increase in residence time for low-FRET to high-FRET transitions (i.e., $T_{\text{low-high}}$), which would likely correspond to DnaJ dissociation events, at the highest concentration of DnaJ tested (10 μM ; Fig. 2C). Conversely, higher concentrations of DnaJ substantially increased the occurrence of transitions between low-FRET states

of Fluc^{IDS} (i.e., $T_{\text{low-low}}$; Fig. 2D); thus, Fluc^{IDS} remains conformationally dynamic but is constrained within an ensemble of non-native and conformationally expanded states when bound to DnaJ. This conformational dynamicity and/or destabilization of Hsp40-bound client proteins have been observed previously, whereby hydrogen deuterium exchange (HDX) experiments demonstrated that amide hydrogens exchange more rapidly upon binding of Fluc by DnaJ (32). Furthermore, a recent study found that the client binding sites on many Hsp40 isoforms span across

the C-terminal subdomain of both Hsp40 protomers within the same dimer (33). Spatial separation of the client across both Hsp40 protomers results in the stabilization of expanded non-native conformations of the client, prevents spontaneous collapse, and may dissolve secondary and tertiary structural elements of the bound client (33), results consistent with this work.

It remains to be established whether DnaJ selectively binds to a subset of already expanded conformations of Fluc^{IDS} (e.g., a conformational selection model) or if binding by DnaJ remodels the conformation of the client protein to expanded states (e.g., an induced fit model) (17, 21, 32, 34–36). To elucidate this, we plotted the frequency of transition distributions as a function of the FRET state before (F_{Before}) and after (F_{After}) each transition as a transition density plot (TDP). When Fluc^{IDS} was incubated in the presence of low concentrations of DnaJ (i.e., $\leq 0.5 \mu\text{M}$), the transition density was predominantly observed at high-FRET values (i.e., 0.6 to 1.0). Conversely, when incubated in the presence of high concentrations of DnaJ (i.e., $> 2 \mu\text{M}$), the transition density shifted to lower-FRET states (i.e., 0.3 to 0.6; Fig. 2E). Notably, the transition distributions are symmetrically mirrored and are close to the TDP diagonal axis at all concentrations of DnaJ tested, which indicates that the observed transitions occur reversibly and are small in amplitude (Fig. 2E and fig. S2B).

Notably, the occurrence of large Fluc^{IDS} conformational changes (> 0.5) does not change with increasing concentrations of DnaJ (fig. S2B), which suggests that DnaJ binding does not typically induce mechanical unfolding of the client. If DnaJ actively induced the conformational expansion of the client, then it would be expected that the residence times of $T_{\text{high-low}}$ transitions would be notably shorter with increasing concentrations of DnaJ (due to increased association rates). However, because the residence times of $T_{\text{high-low}}$ transitions do not change with DnaJ concentration and the TDPs do not demonstrate transition density away from the diagonal axis, our data support a model in which DnaJ scans non-native states and binds to exposed hydrophobic regions typically exposed in already expanded client conformations (37). Although Hsp40 chaperones typically form complexes with their client proteins at a 1:1 ratio (18, 33, 38), the observation that $T_{\text{low-high}}$ residence times are longer in the presence of high concentrations of DnaJ suggests that multiple chaperones can bind to a single misfolded client (because dissociation of individual species is concentration independent). Thus, these data demonstrate that the binding of multiple DnaJ proteins to a single client result in the stabilization of unfolded conformers and partitions the client toward a conformationally expanded ensemble.

DnaK entropically pulls clients to resolve misfolded states

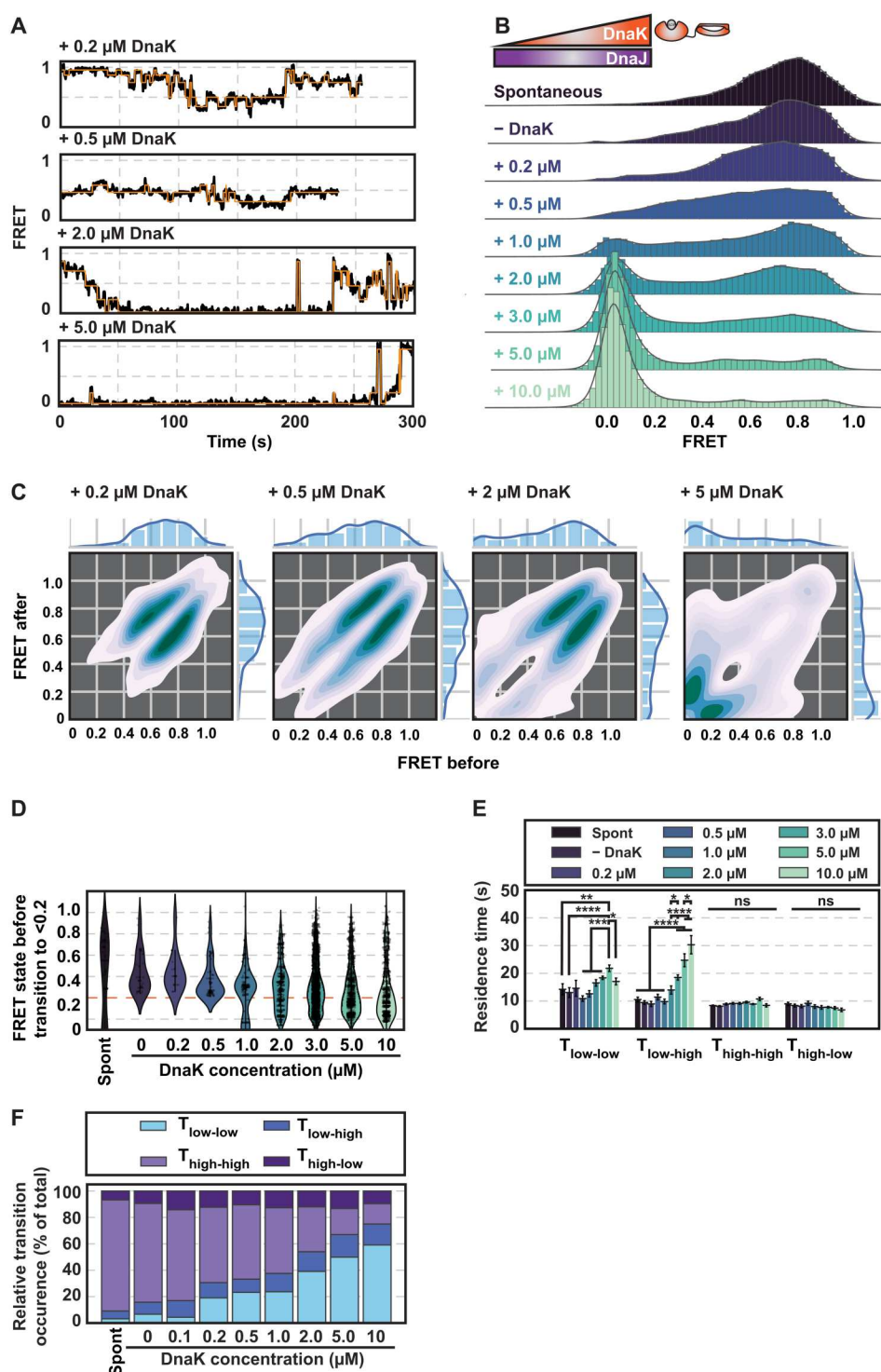
Next, we investigated how DnaJ cooperates with DnaK to fold Fluc^{IDS}. To assess the sole effect of DnaK on the conformation of Fluc^{IDS}, we incubated increasing concentrations of DnaK with a concentration of DnaJ ($0.2 \mu\text{M}$) that alone does not affect the conformation of Fluc^{IDS} but is sufficient to promote DnaK loading onto the client (fig. S2C). Incubation of Fluc^{IDS} with DnaJ only, or when supplemented with a low concentration of DnaK ($0.2 \mu\text{M}$), did not drastically affect the FRET traces or distributions of Fluc^{IDS} (Fig. 3, A and B). Incubation of misfolded Fluc^{IDS} with increasing concentrations of DnaK resulted in the redistribution of high-FRET populations (> 0.5) toward an ultra-lowFRET state (defined as < 0.2) such that, at the highest concentration of DnaK, the ultra-lowFRET peak

constituted $> 70\%$ of the total FRET species. FRET intensity traces from Fluc^{IDS} molecules incubated with higher concentrations of DnaK ($\geq 2 \mu\text{M}$) demonstrate that these ultra-lowFRET states are stable and can persist for minutes (Fig. 3A). As expected, the formation of this ultra-lowFRET state is dependent on the presence of DnaJ and ATP hydrolysis and thus constitutes a DnaK-bound and conformationally expanded form of Fluc^{IDS} (fig. S2C). It is interesting, however, that DnaJ can promote binding of DnaK to Fluc^{IDS} at a DnaJ concentration that by itself is not sufficient to significantly remodel the conformational landscape of Fluc^{IDS}. Such a result suggests that remodeling of the client by DnaJ is not strictly necessary during refolding and that its predominant role is to stimulate ATP hydrolysis and client capture by DnaK; the conformational expansion of the client at high DnaJ concentrations is thus likely a mechanism by which it can prevent the well-described misfolding and subsequent aggregation of Fluc (14, 39). The ultra-lowFRET conformationally expanded conformation of Fluc^{IDS} constitutes a necessary intermediate for chaperone-mediated on-pathway folding, because the absence of ATP from refolding assays inhibits productive Fluc^{IDS} refolding. Collectively, these results demonstrate that the DnaK-bound Fluc^{IDS} molecules are more conformationally expanded compared to DnaJ-bound molecules and contribute to a growing body of literature that conformational expansion of the client is a generic mechanism of Hsp70 function (18–20).

We next interrogated the kinetic data to reveal the mechanism by which DnaK remodels the conformation of clients. Notably, the TDPs demonstrate that there is a clear difference in the mechanism by which DnaK binds to misfolded protein relative to DnaJ. When Fluc^{IDS} was allowed to refold from denaturing in the absence or presence of low concentrations of DnaK ($\leq 0.5 \mu\text{M}$), most transitions occur between high-FRET values (i.e., 0.6 to 1.0) and lay close to the diagonal axis (Fig. 3C). Incubation of Fluc^{IDS} with higher concentrations of DnaK (i.e., $\geq 2 \mu\text{M}$) results in increased transition density at ultra-lowFRET states (e.g., ~ 0 to 0.4). However, and in contrast to those results observed with DnaJ, the TDPs at high concentrations of DnaK exhibited strong transition densities away from the diagonal axis that implies the presence of substantial Fluc^{IDS} conformational changes. High concentrations of DnaK, but not DnaJ, increase the occurrence and proportion of molecules that experience transitions larger in amplitude than 0.5 FRET (fig. S2B). There has been some conjecture regarding the mechanism by which Hsp70 resolves misfolded states of proteins (17–21); thus, we decided to investigate this by quantifying the FRET state of Fluc^{IDS} immediately before a transition to a DnaK-bound state (i.e., < 0.2 FRET; Fig. 3D). Under conditions in which the formation of the DnaK-bound state is favored ($\geq 2 \mu\text{M}$ DnaK), most transitions originate from ultra-lowFRET states. However, a high proportion of transitions originate from high-FRET states (> 0.5), indicating that DnaK can forcibly unfold compact conformations of Fluc^{IDS} (Fig. 3D).

It is interesting that the formation of DnaK-bound Fluc^{IDS} complexes often originated following a single transition from a high-FRET, compact, and misfolded conformation of Fluc^{IDS}. Although the conversion of misfolded Fluc^{IDS} to DnaK-bound states occurred following single transition events, which might suggest the binding of an individual DnaK molecule, it remains possible that multiple DnaK species associate with Fluc^{IDS} because only one structural coordinate can be monitored using conventional two-color smFRET.

Fig. 3. DnaK resolves misfolded states of Fluc^{IDS} by conformational expansion. Fluc^{IDS} was diluted from denaturant in the absence (i.e., spontaneous) or presence of DnaJ (0.2 μ M), and increasing concentrations of DnaK (0 to 10 μ M) and the FRET efficiency were measured. ATP (5 mM) was present for all conditions tested. (A) Representative smFRET traces of individual Fluc^{IDS} molecules when incubated in the presence of DnaJ and the indicated concentration of DnaK. Additional traces are shown in fig. S5. (B) Ridgeline plot of the FRET efficiency distributions of misfolded Fluc^{IDS} or when incubated with DnaJ and the indicated concentration of DnaK. (C) TDPs showing Fluc^{IDS} transitions when incubated in the presence of DnaJ and the indicated concentration of DnaK. (D) Violin plot of the FRET efficiencies of Fluc^{IDS} molecules immediately preceding a transition (i.e., F_{Before}) to an ultra-low FRET state (<0.2). (E) Bar plots showing the residence time of different transition classes. A two-way ANOVA statistical analysis with Tukey's multiple-comparisons post hoc test was performed to determine statistically significant differences in residence times between treatment groups within each transition class. * $P \leq 0.05$, ** $P \leq 0.01$, *** $P \leq 0.001$, and **** $P \leq 0.0001$. ns or the absence of markers indicates no significant difference ($P > 0.05$). (F) The relative transition occurrence of each transition class. Data for all panels were derived and collated from the HMM fits of at least 155 individual Fluc^{IDS} molecules per treatment.



Considering that the dissociation of a single DnaK species from Fluc^{IDS} is concentration independent (18), the kinetic data support a model by which multiple DnaK species are bound to Fluc^{IDS} because the apparent dissociation of DnaK from Fluc^{IDS} is significantly slower with increasing concentrations of DnaK (as indicated by longer residence times for $T_{\text{low-high}}$ transitions; see Fig. 3E and Methods). Notably, when the residence times of those

transitions that originate from or to DnaK-bound states (i.e., <0.2 FRET) were determined, a twofold reduction in residence time was observed for $T_{\text{high-low}}$ transitions (fig. S2D). These data demonstrate that the loading of multiple DnaK molecules onto a single client is promoted by increased association rates at high chaperone concentrations, consistent with reports that have shown that up to 12 DnaK species can bind to a single client protein (18, 19). To provide a

more quantitative measure of the frequency of certain transitions above that provided by the TDP analysis, we interrogated the relative occurrence of each transition class (Fig. 3F). Notably, higher concentrations of DnaK further increase the abundance of transitions constrained at low-FRET efficiencies (i.e., $T_{\text{low-low}}$ transitions), while the converse was true for $T_{\text{high-high}}$ transitions. Consequently, once bound by DnaK, Fluc^{IDS} is unlikely to transition from a low-FRET state (<0.5) to a high-FRET state (>0.5; fig. S2E) but remains conformationally dynamic while constrained in the expanded ensemble. Collectively, these kinetic analyses support an entropic pulling mechanism, whereby the rapid association and subsequent repulsion of multiple DnaK species bound to a single client result in its mechanical unfolding, partitioning the client toward conformationally expanded states.

Multiple cycles of DnaK binding and release are essential for productive folding and are exquisitely regulated by GrpE concentration

The conformation of Fluc^{IDS} as it is folded by the complete KJE system was then assessed. As expected, incubation of misfolded Fluc^{IDS} with DnaJ and DnaK in the absence of GrpE resulted in a shift to the ultra-low FRET state characteristic of DnaK-bound Fluc^{IDS} (Fig. 4, A and B, and fig. S6A). Consistent with the role of GrpE to dissociate ADP and promote client release from DnaK (14, 40–42), the addition of increasing concentrations of GrpE resulted in the DnaK-bound state of Fluc^{IDS} becoming less abundant with Fluc^{IDS} instead occupying FRET distributions typical of native (~0.6) or misfolded (~0.8) states. Notably, Alexa Fluor 555 (AF555)/AF647-labeled Fluc^{IDS} that had been refolded by the KJE system in bulk and was confirmed to be enzymatically active also occupied FRET states identical to that of native protein before unfolding (fig. S7, A and B). This observation indicates that the native-like populations observed in this treatment represent correctly folded Fluc^{IDS} species. Furthermore, Fluc^{IDS} molecules conjugated to streptavidin-functionalized microplate wells could be refolded by the KJE system to an enzymatically active state, demonstrating that immobilization of Fluc^{IDS} to a surface does not impair its ability to be refolded by chaperones (fig. S7, C and D).

To quantify the effect of GrpE concentration on Fluc^{IDS} refolding, we determined the relative proportion of DnaK-bound, native, and misfolded Fluc^{IDS} populations by fitting the histogram data with a multiple Gaussian model (Fig. 4C and fig. S8A). As expected, the proportion of DnaK-bound Fluc^{IDS} species was observed to decrease with increasing concentrations of GrpE; however, misfolded Fluc^{IDS} species became notably more abundant. Such a result is consistent with the destabilization of DnaK-Fluc^{IDS} complexes by GrpE, as evidenced by the significantly reduced residence times and transition frequencies of DnaK-bound states (i.e., $T_{\text{low-low}}$ and $T_{\text{low-high}}$) compared to those in the absence of GrpE (fig. S8, B and C). The proportion of native Fluc^{IDS} molecules increased until a maximum of 45% was reached at intermediate GrpE concentrations (i.e., 2 μM) but decreased at higher concentrations (Fig. 4C).

Such a result suggests that during KJE-mediated refolding, there is a compromise between preventing the accumulation of misfolded species and effectively refolding the client to its native state. To interrogate this further, we determined the change in Fluc^{IDS} populations when incubated with low or intermediate concentrations of GrpE ($\leq 2 \mu\text{M}$) during refolding (Fig. 4D). Low concentrations of GrpE (0.5 μM) delays the opportunity for the client to fold upon

chaperone release (as indicated by a high proportion of DnaK-bound states) but reduces the proportion of misfolded species (due to higher DnaK-Fluc^{IDS} affinity): Refolding of Fluc^{IDS} to the native state occurs over time but is slow and inefficient, with only 38% of Fluc^{IDS} species occupying native-like FRET distributions. Conversely, intermediate concentrations of GrpE (2 μM) results in the rapid dissociation of DnaK-bound Fluc^{IDS} species, which allows the client an early opportunity to fold correctly. Notably, a high proportion of misfolded protein is generated immediately following initial DnaK release; however, over time, the misfolded population is partitioned toward native Fluc^{IDS} states that become the predominant species at later time points.

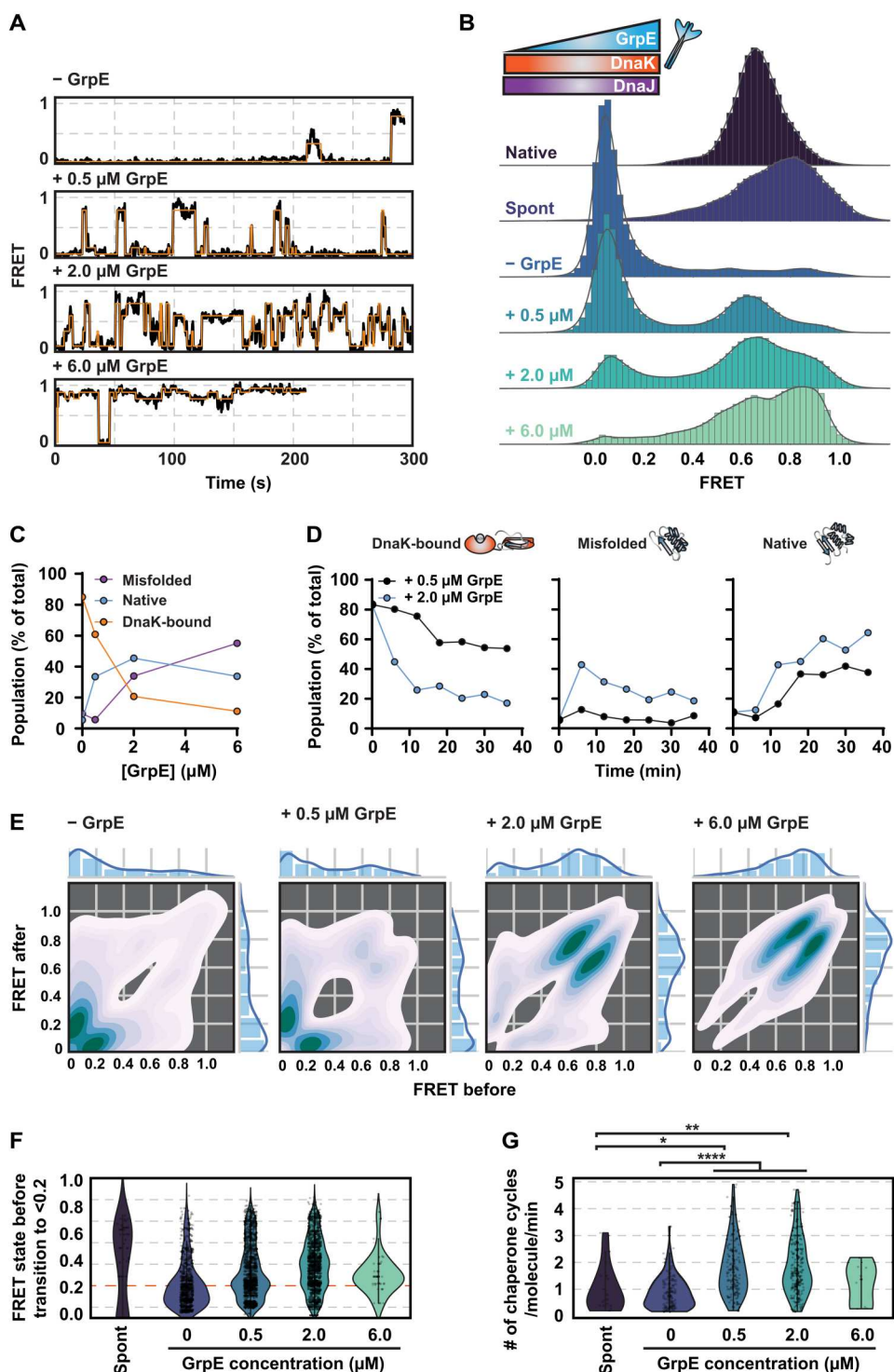
These data also suggest that the ability of DnaK to inhibit refolding of luciferase at high concentrations (13) occurs as a result of non-optimal ratios of the chaperones, whereby limiting concentrations of GrpE promote the accumulation of DnaK onto clients and reduce opportunities for refolding. To interrogate this further, we performed refolding assays in which the concentration of DnaK was titrated to very high concentrations (e.g., 50 μM , thereby substantially increasing the amount of DnaK bound to the client). We observed that the yield and rate of Fluc^{IDS} refolding decreased at higher concentrations of DnaK (>2 μM ; fig. S9, A and B). However, at these concentrations of DnaK where refolding was inhibited (e.g., 20 μM), this DnaK-mediated inhibition could be overcome by the addition of increasing concentrations of GrpE (>1 μM ; fig. S9, C and D). Collectively, the smFRET and enzyme-activity data indicate that conditions in which entropic pulling occurs (e.g., high concentrations of DnaK) are favorable for protein folding provided that the dissociation rates are sufficiently high to allow client refolding upon DnaK dissociation. Refolding is reliant on the conformational expansion of misfolded states, which is facilitated by entropic pulling, and, hence, the two processes (i.e., folding and entropic pulling) are not mutually exclusive.

The current description of chaperone-mediated folding suggests that, should the released client remain misfolded, it can undergo additional rounds of chaperone-mediated binding and release (21, 43–46). In this work, multiple cycles of chaperone binding and release of a single client protein were observed in real time during chaperone-assisted refolding. Many Fluc^{IDS} molecules exhibited repeated transitions to and from ultra-low FRET states when incubated with lower concentrations of GrpE ($\leq 2 \mu\text{M}$; >70%; Fig. 4A; and figs. S6, B and C, and S8D), indicative of multiple cycles of DnaK binding and release. Accordingly, the TDP analysis demonstrated substantial transition density away from the diagonal axis under these experimental conditions (Fig. 4E). Furthermore, a large proportion of transitions to DnaK-bound states (i.e., <0.2) were observed to originate from high-FRET misfolded Fluc^{IDS} conformations (>0.5) during refolding (Fig. 4F); such a result supports the TDP analyses and further demonstrates that DnaK can bind to and unfold a variety of misfolded Fluc^{IDS} structures during productive folding. In contrast, very few Fluc^{IDS} molecules experienced transitions to ultra-low FRET states when refolded in the presence of high concentrations of GrpE (6 μM ; <10%; Fig. 4A and figs. S6D and S8D), with the transition density focused in high-FRET regimes along the diagonal axis of the TDP (Fig. 4E).

To ascertain whether multiple chaperone cycles actively promote efficient protein folding, we calculated the rate of DnaK binding and release to individual client proteins (see Methods and Fig. 4G). Under conditions in which Fluc^{IDS} refolding is promoted and

Fig. 4. GrpE promotes efficient Fluc^{IDS} refolding by enabling multiple cycles of DnaK binding and release.

Fluc^{IDS} was incubated in the presence of DnaJ (0.6 μ M), DnaK (9 μ M), and ATP (5 mM) supplemented with increasing concentrations of GrpE (0 to 6 μ M). FRET efficiency data are measured for 36 min following the addition of GrpE. (A) Representative smFRET traces of individual Fluc^{IDS} molecules when incubated in the presence of chaperones. Additional traces are shown in fig. S6. (B) Ridgeline plot of the FRET efficiency distributions of native or misfolded Fluc^{IDS} or when incubated with DnaJ, DnaK, and the indicated concentration of GrpE. (C) Proportion of Fluc^{IDS} states (i.e., either DnaK-bound, native, or misfolded) as a function of GrpE concentration. (D) Proportion of Fluc^{IDS} states over time when incubated in the presence of either 0.5 or 2 μ M GrpE. (E) TDPs showing Fluc^{IDS} transitions when incubated in the presence of DnaJ, DnaK, and the indicated concentration of GrpE. (F) Violin plots of the FRET efficiencies of Fluc^{IDS} molecules immediately preceding a transition (i.e., F_{Before}) to an ultra-low FRET state (<0.2). (G) Violin plots showing the distribution of chaperone binding and release events to individual Fluc^{IDS} molecules per minute in the presence of different concentrations of GrpE. A binding event was classified if F_{Before} and F_{After} were greater than and less than 0.2 FRET, respectively, and vice versa for release events. A one-way ANOVA statistical analysis with Tukey's multiple-comparisons post hoc test was performed to determine statistically significant differences in the rate of chaperone binding and release events between treatment groups. When statistical tests were performed, * $P \leq 0.05$, ** $P \leq 0.01$, *** $P \leq 0.001$, and **** $P \leq 0.0001$. ns or the absence of markers indicates no significant difference ($P > 0.05$). Data for all panels were derived and collated from the HMM fits of at least 205 individual Fluc^{IDS} molecules per treatment.



misfolding is minimized (i.e., ≤ 2 μ M GrpE), the rate of chaperone binding and release events per molecule was observed to be significantly higher compared to when refolding is inefficient (i.e., in the absence of GrpE). Furthermore, under conditions in which only a single binding and release event per molecule is possible (i.e., upon dissociation of DnaK bound to Fluc^{IDS} and its subsequent removal from solution upon incubation with GrpE only), no Fluc^{IDS}

refolding was observed (fig. S8E). Notably, addition of only GrpE to DnaK-client complexes results in an immediate return to high-FRET states, indicating that GrpE-mediated dissociation of DnaK results in spontaneous collapse of the client from expanded conformations (fig. S8F). These results illustrate that multiple cycles of chaperone binding and release are essential for productive Fluc^{IDS} refolding.

This work sought to address the outstanding question of how the Hsp70 chaperone system promotes client refolding. To do so, we developed a Fluc construct in which the folded state can be monitored with temporal resolution using a combination of TIRF microscopy and smFRET. We have observed the conformation of an individual client protein in real time as it passes through the entire Hsp70 functional cycle and extracted key kinetic and structural details that are typically inaccessible using conventional approaches.

The mechanism by which molecular chaperones interact with clients and affect their conformation is considered central to chaperone function. We show that, unlike DnaK, the binding of multiple DnaJ species to a single client does not result in entropic pulling but instead prevents the collapse of Fluc^{IDS} to misfolded compact conformations. What then could be the difference in fold stabilization between these two chaperones? One hypothesis could be that binding of multiple DnaJ species to a single client stabilizes the unfolded conformers; however, because Hsp40 chaperones typically bind to their clients via many weak, low-affinity, and multivalent interactions (33), any instances of steric clashing or kinetic competition between DnaJ molecules for binding sites could accelerate the dissociation of DnaJ species partially bound to Fluc^{IDS}. Conversely, DnaK is a non-equilibrium machine that uses ATP hydrolysis to bind clients, which results in an apparent affinity for the client that is significantly higher than can be achieved by the ADP-bound form of DnaK alone (a concept referred to as ultra-affinity) (47). Because dissociation of DnaK is dependent on ADP release, which is rate-limiting in the absence of an NEF, steric clashes between bound DnaK species inherently lead to repulsion of the two chaperones and result in the mechanical unfolding of the client. This model is consistent with previous theoretical work and computational simulations that propose the ultra-affinity of DnaK for the client is essential in converting energy into mechanical work via entropic pulling (48). In addition, we were able to directly observe this phenomenon at the single-protein level because complete conformational expansion of the client was observed to occur in a single event (i.e., no intermediate states are required on the way to the ultra-low FRET state). These events occurred more frequently under conditions where binding of multiple DnaK species to a single client are favored (e.g., high concentrations of DnaK), which further validates the entropic pulling model of Hsp70 function. Together, it is apparent that the relative affinities of DnaJ and DnaK for binding to the client dictate the mechanism by which they affect its conformational landscape; lower affinities favor a conformational selection mechanism, while high affinities favor an entropic pulling model. By directly observing the conformational dynamics of individual clients upon interaction with molecular chaperones over time, which has typically been inaccessible using other ensemble or single-molecule confocal-based approaches (18, 19, 33), we have been able to validate the mechanisms by which these different chaperone classes interact with their clients. The findings of this study, as well as others (19, 21, 49), show that the entropic pulling of client proteins by DnaK helps to resolve folding-incompetent, misfolded structures and that chaperones can conformationally remodel the client for subsequent refolding attempts.

It is traditionally thought that the release of the client protein from Hsp70 provides an opportunity for the client to spontaneously refold to the native state. Recent work has suggested that the role of Hsp70 is to resolve misfolded Fluc states and unfold it (i.e.,

“unfoldase” activity), following which the client can spontaneously refold to the native state upon release by Hsp70 (i.e., similar to denaturant-induced refolding) (21). However, the results of this work suggest that the unfoldase mechanism of Hsp70 chaperone function may not fully encompass its role in protein folding and that Hsp70 has “foldase” characteristics. As evidence for this, the rate of chaperone-assisted refolding of Fluc^{WT} was ~4-fold faster than that observed for Fluc^{IDS}; however, the spontaneous refolding efficiency of Fluc^{WT} was ~10-fold higher than for Fluc^{IDS}. This suggests that the chaperone-assisted refolding mechanism extends beyond simple release of an unfolded client protein for spontaneous refolding and that there is some other aspect of chaperone function that accelerates and assists productive folding.

There is a growing body of work that suggests that Hsp70 can direct the folding of proteins in a manner that is distinct from a simple model of binding and release (20, 50–52). Kinetic data obtained in this work demonstrated that there was a much lower probability that Fluc^{IDS} would return to high-FRET compacted states once conformationally expanded by Hsp70, indicative of some “holdase”-like function. Notably, it has been suggested that the binding of Hsp70 to multiple sites on the client resolves different misfolded structures and may enable the client to occupy heterogeneous and “fuzzy” ensemble structures at regions distinct from the binding site; these structures can subsequently act as folding nuclei that allow the client to explore numerous folding pathways upon chaperone release (20, 21, 46, 50, 51). Furthermore, molecular dynamics simulations suggests that Hsp70 may remain transiently associated with the released client and prevent non-native contacts to accelerate productive refolding (52). While more work is required to validate these hypotheses in the context of Fluc^{IDS} folding, it is clear that Hsp70 can actively remodel the folding landscape of its clients by partitioning them toward native structures and away from non-productive folding pathways.

The kinetic data provide convincing evidence that the refolding efficiency is exquisitely dependent on GrpE concentration and is dictated by several key parameters: (i) the relative affinity of DnaK to misfolded Fluc^{IDS} and (ii) the number and rate of DnaK binding and release cycles per molecule. Here, the benefit of visualizing the conformation of client proteins temporally during chaperone-assisted folding is clear, since multiple chaperone binding and release events to a single client protein could be directly observed and the kinetics characterized. These data demonstrate that even low concentrations of GrpE promote many rapid cycles of DnaK binding and release to the client. However, under these conditions, the relative affinity of DnaK to Fluc^{IDS} is high (because of slower nucleotide exchange rates), which results in the accumulation of DnaK onto misfolded Fluc^{IDS} and reduces opportunities for spontaneous refolding. Conversely, high concentrations of GrpE reduces the amount of productive DnaK binding events and thus the number and rate of chaperone binding and release events. Thus, refolding is most effective in the presence of intermediate concentrations of GrpE, i.e., when the rate and occurrence of DnaK binding and release are high, while the relative affinity of DnaK to Fluc^{IDS} remains low. While others have suggested that multiple chaperone cycles are required for productive folding (14, 21, 35, 53), here, we provide conclusive evidence that multiple cycles facilitate significant conformational remodeling of misfolded clients and allow additional opportunities for correct folding to occur and that faster

rates of binding and release correlate with improved yields and rates of refolding.

Collectively, the results described in this work provide a detailed understanding of the mechanism by which the bacterial Hsp70 chaperone system refolds client proteins. Capture of the client by DnaK occurs upon DnaJ-assisted ATP hydrolysis (generating the ADP-bound form of DnaK), which actively drives additional conformational expansion and global unfolding of the bound client via entropic pulling. At this stage, the client remains conformationally dynamic and may form native contacts in regions distinct from the binding site to prepare for refolding upon DnaK release. Dissociation of ADP from DnaK, which can occur spontaneously but is accelerated by a NEF, results in the concomitant rebinding of ATP and dissociation of the client protein from DnaK. Upon release, DnaK can partition the client protein toward folding pathways en route to the native state, or the client can spontaneously misfold. The misfolded protein can then be subject to additional rounds of binding and release by chaperones until the native state is acquired. The results of this work further demonstrate that the rate at which chaperone binding and release events occur to a single client is a critical factor in efficient refolding.

METHODS

Materials

Recombinant Fluc^{WT} was purchased from Sigma-Aldrich (Missouri, USA). Plasmids encoding glutathione *S*-transferase (GST)-tagged Fluc mutants were donated by T. Böcking (University of New South Wales, Australia). A N-terminal small ubiquitin-like modifier (SUMO) solubility tag and a C-terminal AviTag were added to the Fluc mutant through standard cloning procedures, with the SUMO-tag replacing the N-terminal GST-tag. Plasmids encoding KJE chaperones were donated by M. Mayer (University of Heidelberg, Germany).

Expression and purification of recombinant protein Fluc^{IDS}

Escherichia coli BL21(DE3) cells cotransformed with plasmids encoding biotin ligase (BirA) and Fluc^{IDS} (with N-terminal 6x-His-SUMO and C-terminal AviTag motifs) were used to inoculate a starter culture consisting of LB medium supplemented with kanamycin (50 µg/ml) and chloramphenicol (10 µg/ml) and grown overnight at 37°C with constant agitation at 180 rpm in an orbital shaker. The starter culture was used to inoculate expression cultures containing LB medium supplemented only with kanamycin (50 µg/ml), and the cultures were incubated at 37°C until an optical density at 600 nm (OD₆₀₀) of ~0.4 was reached. Expression cultures were then further incubated at 18°C until an OD₆₀₀ of ~0.6 to 0.8 was reached. To promote the *in vivo* biotinylation of the AviTagged recombinant protein, the medium was supplemented with D-biotin (50 µM final concentration) prepared in 10 mM bicine buffer (pH 8.3) before protein induction. The expression of recombinant protein was induced by addition of isopropyl-β-D-1-thiogalactopyranoside (IPTG; 0.1 mM), with the cultures incubated on an orbital shaker at 130 rpm overnight (~20 hours) at 18°C. The cells were then harvested by centrifugation at 5000g for 10 min at 4°C, and the pellet was stored at –20°C until the recombinant protein was extracted.

Recombinant Fluc^{IDS} was extracted from the bacterial pellet via resuspension in 50 mM tris-HCl (pH 8.0) supplemented with 300 mM NaCl, 5 mM imidazole, 10% (v/v) glycerol [immobilized metal-affinity chromatography (IMAC) buffer A] that also contained lysozyme (0.5 mg/ml), and EDTA-free cocktail protease inhibitor. The resuspended pellet was then incubated at 4°C for 20 min, and the lysates subjected to probe sonication for 3 min (10-s on/20-s off) at 45% power. The cell debris was then pelleted twice at 24,000g for 20 min at 4°C, and the soluble bacterial lysate passed through a 0.45-µm filter to remove particulates before subsequent purification.

The lysate containing recombinant Fluc^{IDS} (with N-terminal 6x-His-SUMO tag) was loaded onto a 5-ml His-Trap Sephadex column equilibrated in IMAC buffer A and bound protein eluted with IMAC buffer A supplemented with 500 mM imidazole (IMAC buffer B). Fractions containing eluted protein were pooled and dialyzed overnight at 4°C in the presence of ubiquitin-like-specific protease (Ulp1, 4 µg/mg of recombinant protein) against IMAC buffer A that did not contain imidazole (IMAC buffer C). Recombinant Fluc^{IDS} was further purified away from contaminant proteins and the cleaved SUMO tag by passing the dialysate over the same His-Trap Sephadex IMAC column equilibrated in IMAC buffer C and was purified as previously described; however, this time, the recombinant protein did not bind to the column and so was collected in flow through fractions. Fractions containing recombinant protein were pooled and dialyzed into 10 mM tris (pH 9.0) supplemented with 0.5 mM EDTA and 10% (v/v) glycerol [ion-exchange (IEX) buffer A] for further purification by IEX chromatography. Dialyzed protein was loaded onto a MonoQ 5/50 column equilibrated in IEX buffer A. Recombinant Fluc^{IDS} was eluted from the column using a linear salt gradient (0 to 300 mM NaCl) over 20 column volumes. Eluate fractions containing recombinant protein were pooled and dialyzed into storage buffer [50 mM tris (pH 7.5) and 10% (v/v) glycerol], concentrated, snap-frozen in liquid nitrogen, and stored at –80°C until required.

Molecular chaperones

BL21(DE3) *E. coli* cells transformed with plasmid encoding bacterial chaperones (i.e., KJE) were used to inoculate a starter culture consisting of LB medium supplemented with the appropriate antibiotic [kanamycin (50 µg/ml) for DnaK and DnaJ and ampicillin (100 µg/ml) for GrpE] and grown overnight at 37°C. The cultures were used to inoculate expression cultures containing LB medium with the appropriate antibiotic and were grown at 37°C to the required OD₆₀₀ (0.8 for DnaK and 1.2 for DnaJ or GrpE). Recombinant protein expression was induced upon the addition of 1 mM IPTG (for DnaK or DnaJ) or 0.2% (w/v) L-(+)-arabinose (for GrpE), and cells were harvested following 4 hours of shaking at 30°C. The bacterial pellets were resuspended in protein-specific lysis buffers [DnaK: 20 mM tris (pH 7.9), 100 mM KCl, and 20 mM imidazole; DnaJ: 50 mM tris (pH 7.9), 500 mM NaCl, 0.1% (v/v) Triton X-100, and 5 mM MgCl₂; GrpE: 20 mM tris (pH 7.9), 100 mM NaCl, and 5 mM MgCl₂] that also contained lysozyme (0.5 mg/ml) and EDTA-free cocktail protease inhibitor. Recombinant protein was extracted and the lysate was clarified, as described above for Fluc^{IDS}.

All proteins were purified using IMAC. Briefly, the lysate containing recombinant DnaK was passed over an IMAC column equilibrated in the appropriate lysis buffer and washed in lysis buffer supplemented first with 20 mM imidazole and then with 5 mM

ATP and 5 mM MgCl₂. Bound protein was eluted in lysis buffer supplemented with 250 mM imidazole, with bound fractions pooled and dialyzed against lysis buffer in the presence of Ulp1 (4 μg/mg of recombinant protein) to remove the N-terminal 6x-His-SUMO tag. The dialysate was then passed onto the IMAC column a second time and purified as described above, with fractions containing recombinant protein pooled, dialyzed into storage buffer [40 mM Hepes-KOH (pH 7.6), 100 mM KCl, 5 mM MgCl₂, 10 mM β-mercaptoethanol (BME), and 10% (v/v) glycerol], and stored at –80°C until use. Recombinant GrpE was purified as described above for DnaK, with the exception that the GrpE lysis buffer was used instead of the DnaK lysis buffer and recombinant GrpE was dialyzed into 40 mM Hepes-KOH (pH 7.6) supplemented with 150 mM NaCl and 10% (v/v) glycerol for storage at –80°C.

DnaJ was purified as described for DnaK using the appropriate lysis buffer with the following modifications. Lysate containing recombinant DnaJ was loaded onto an IMAC column equilibrated in the appropriate lysis buffer and washed in lysis buffer supplemented first with 1.5 M NaCl and then supplemented with 200 mM NaCl. Bound protein was then eluted in lysis buffer supplemented with 250 mM imidazole and 200 mM NaCl, with bound fractions pooled and dialyzed against lysis buffer in the presence of Ulp1 (4 mg in total) to remove the N-terminal 6x-His-SUMO tag. The dialysate was then passed onto the IMAC column a second time and purified as described above, with fractions containing recombinant protein pooled, dialyzed into storage buffer [40 mM Hepes-KOH (pH 7.6), 300 mM KCl, and 10% (v/v) glycerol], and stored at –80°C until use.

Refolding assays

The ability of denatured Fluc^{IDS} to spontaneously refold to a native state was assessed by measuring the return of enzymatic activity after denaturation. Denatured Fluc^{IDS} was prepared by incubation of native Fluc^{IDS} in unfolding buffer [50 mM Hepes-KOH (pH 7.5), 50 mM KCl, 5 mM MgCl₂, 2 mM dithiothreitol (DTT), and 5 M GdHCl] for 30 min at room temperature. Spontaneous refolding of denatured Fluc^{IDS} was initiated by a 1:100 dilution into refolding buffer [50 mM Hepes-KOH (pH 7.5), 80 mM KCl, 5 mM MgCl₂, 2 mM DTT, and 0.05% (v/v) Tween 20] such that the final concentration of Fluc^{IDS} was 10 nM. Refolding reactions with bacterial chaperones (i.e., KJE system) were left to incubate at 25°C for up to 90 min. Throughout the refolding reactions, aliquots were taken at various times and dispensed into the bottom of a white 96-well Costar plate (Sigma-Aldrich, USA). The luminescence reaction was initiated following injection of a 10-fold excess of assay buffer [25 mM glycylglycine (pH 7.4), 0.25 mM luciferin, 100 mM KCl, 15 mM MgCl₂, and 2 mM ATP] into a single well, and 5 s after injection, the luminescence was measured for 10 s using a POLARstar Omega (BMG Labtech, Germany) plate reader. The injection and measurement procedure described above was then performed sequentially for each well to ensure consistency between the measurements. All measurements were performed at 25°C with the gain set to 4000. Refolding yields were calculated by normalizing to the activity of native (non-denatured) Fluc^{IDS}, which was treated as described above with the exception that GdHCl was omitted from the unfolding buffer.

Chaperone-assisted refolding reactions were performed as described above with the exception that denatured Fluc^{IDS} was diluted into refolding buffer containing chaperones and nucleotide.

Briefly, refolding assays containing bacterial chaperones were performed with either Fluc^{IDS} or Fluc^{WT} in the presence of 1 μM DnaJ, 3 μM DnaK, and 1.5 μM GrpE (when present) supplemented with either 2 or 5 mM ATP. To monitor the KJE-assisted refolding of misfolded Fluc^{IDS}, following 60 min of unassisted refolding (i.e., spontaneously refolded treatment), an aliquot of Fluc^{IDS} was diluted 10-fold (1 nM final concentration) into refolding buffer containing the KJE chaperone system, and the luminescence was measured at various time points.

To determine whether DnaK-mediated inhibition of refolding could be ameliorated by GrpE, refolding experiments were performed as described above in the presence of DnaJ (0.2 μM), GrpE (1 μM), and ATP (5 mM) and varying concentrations of DnaK (0 to 50 μM). On the basis of the results of these assays, GrpE titration experiments (0 to 20 μM) were performed in the presence of DnaJ (0.2 μM) and ATP (5 mM), and a concentration of DnaK (20 μM) that was observed to inhibit refolding. The refolding of AF555/AF647-labeled Fluc^{IDS} (1 nM final concentration) was performed as described above in the absence or presence of the KJE system (0.2 μM DnaJ, 3 μM DnaK, and 2 μM GrpE). Last, the ability of the KJE system to refold Fluc^{IDS} that had been specifically immobilized to a streptavidin-functionalized surface was assessed using white, 96-well Pierce streptavidin-coated high-capacity plates. Wells were washed in refolding buffer according to the manufacturer's instructions and incubated with 100 μl of Fluc^{IDS} (500 pM) for 30 min at 25°C. Wells were then washed 3× with refolding buffer. To generate denatured Fluc^{IDS}, wells containing immobilized Fluc^{IDS} were incubated in refolding buffer supplemented with 4 M GdHCl and incubated for 5 min at 25°C. To initiate refolding, all buffers were removed from the wells and replaced with 100 μl of refolding buffer supplemented with the indicated concentration of chaperones or a non-chaperone control protein, ovalbumin. As a control for the specific immobilization of Fluc^{IDS}, the immobilization process was repeated as described above with wells that had been pre-incubated with D-biotin (20 mM) in refolding buffer before the addition of native Fluc^{IDS}. At the designated time points, 100 μl of assay buffer was directly injected into the refolding reaction and luminescence measured as described previously.

All data were fit to a one-phase association or sigmoidal curve to determine the maximum refolding yield (denoted as Y_{max}), and the time required to achieve half Y_{max} (denoted as $t_{1/2}$) was calculated using GraphPad Prism 9 software. For the DnaK and GrpE titration experiments, the rate of refolding was calculated by taking the refolding yield at $t_{1/2}$ and dividing by $t_{1/2}$.

TIRF microscopy Protein labeling

Fluc^{IDS} was fluorescently labeled with an AF555 and AF647 FRET pair as described previously [Kim *et al.* (54)] with minor modifications. Briefly, Fluc^{IDS} (2 mg/ml) was incubated in the presence of 5 mM tris(2-carboxyethyl)phosphine and 40% (w/v) ammonium sulfate and placed on a rotator for 1 hour at 4°C. Proteins were then centrifuged at 20,000g for 15 min and resuspended in degassed buffer A [100 mM Na₂PO₄ (pH 7.4), 200 mM NaCl, 1 mM EDTA, and 40% (w/v) ammonium sulfate]. The protein was then centrifuged at 20,000g for 15 min and resuspended in degassed buffer B [100 mM Na₂PO₄ (pH 7.4), 200 mM NaCl, and 1 mM EDTA]. Fluc^{IDS} was then incubated in the presence of a four- and sixfold excess of pre-mixed AF555 donor and AF647 acceptor

fluorophores, respectively, and placed on a rotator overnight at 4°C. Following the coupling reaction, excess dye was removed by gel filtration chromatography using a 7000 molecular weight cutoff Zeba Spin Desalting column (Thermo Fisher Scientific, USA) equilibrated in 50 mM Tris (pH 7.5) supplemented with 20% (v/v) glycerol. The concentration and degree of labeling were calculated by ultraviolet absorbance.

Microscope setup

Samples were imaged using a custom-built TIRF microscopy system constructed using an inverted optical microscope (Nikon Eclipse TI) that was coupled to an electron-multiplied charge-coupled device (EMCDD) camera (model C9100-13, Hamamatsu Photonics K.K., Japan). The camera was integrated to operate in an objective-type TIRF setup with diode-pumped solid-state lasers (200-mW sapphire; Coherent, USA) emitting circularly polarized laser radiation of 488-, 532-, or 647-nm continuous wavelength. The laser excitation light was reflected by a dichroic mirror (ZT405/488/532/640, Semrock, USA) and directed through an oil immersion objective lens (CFI Apochromate TIRF Series 60× objective lens, numerical aperture = 1.49) and onto the sample. Total internal reflection was achieved by directing the incident ray onto the sample at an angle at the critical angle (θ_c) of $\sim 67^\circ$ for a glass/water interface. The evanescent light field generated selectively excites the surface-immobilized fluorophores, with the fluorescence emission passing through the same objective lens and filtered by the same dichroic mirror. The emission was then passed through a 635-nm long-pass filter (BLP01-635R, Semrock, USA), and the final fluorescent image was projected onto the EMCDD camera. The camera was running in-frame transfer mode at 20 Hz, with an electron multiplication gain of 700, operating at -70°C with a pixel distance of 110 nm (in the sample space).

Coverslip preparation and flow cell assembly

Coverslips were functionalized with neutravidin as previously described (55), with minor modifications. Briefly, 24-mm by 24-mm glass coverslips were cleaned by alternatively sonicating in 100% ethanol and 5 M KOH for a total of 2 hours before aminosilanization in 2% (v/v) 3-aminopropyl trimethoxysilane (Alfa Aesar, USA) for 15 min. *N*-hydroxysuccinimide-ester methoxy-polyethylene glycol, molecular weight of 5 kDa (mPEG), and biotinylated mPEG (bPEG; Laysan Bio, USA), at a 20:1 (w/w) ratio, were dissolved in 50 mM 4-morpholinepropanesulfonic acid (pH 7.4) buffer and sandwiched between two activated coverslips for a minimum of 4 hours for initial passivation in a custom-made humidity chamber. PEGylated coverslips were then rinsed with Milli-Q and PEGylated again as described above for overnight (~ 20 hours) passivation. PEGylated coverslips were rinsed with Milli-Q water, dried under nitrogen gas, and stored at -20°C until required. Before use, neutravidin (0.2 mg/ml; BioLabs, USA) in Milli-Q was incubated on the passivated coverslip for 10 min to bind to the bPEG. Neutravidin-functionalized coverslips were then rinsed with Milli-Q, dried under nitrogen gas, and bonded to a polydimethylsiloxane flow cell for use in single-molecule experiments. Last, to reduce the non-specific binding of proteins to the coverslip surface, each channel in the microfluidic setup was incubated in the presence of 2% (v/v) Tween 20 for 30 min as previously described (56) and then washed with imaging buffer [50 mM Tris (pH 7.5), 80 mM KCl, 10 mM MgCl₂, 200 mM BME, and 6 mM 6-hydroxy-2,5,7,8-tetramethylchroman-2-carboxylic acid (Trolox)].

Surface immobilization of labeled proteins and acquisition of smFRET data

For smFRET experiments, labeled Fluc^{IDS} was specifically immobilized to a neutravidin-functionalized and Tween 20-coated coverslip. To do so, labeled protein (~ 50 pM final concentration) was diluted in imaging buffer and incubated in the flow cell for 5 min. These conditions would typically give rise to ~ 200 to 300 FRET-competent molecules per 100- μm by 100- μm . Unbound proteins were then removed from the flow cell by flowing through imaging buffer.

All data were acquired using the TIRF microscope setup previously described following sample illumination using a 532-nm solid-state laser with excitation intensity of 2.6 W/cm², and the fluorescence of donor and acceptor fluorophores was measured every 200 or 500 ms (for GdHCl-induced folding and unfolding experiments) at multiple fields of view. An oxygen scavenging system consisting of 5 mM protocatechuic acid and 50 nM protocatechuate-3,4-dioxygenase was included in all buffers before and during image acquisition to minimize photobleaching and fluorophore blinking.

smFRET data experiments

Characterization of the Fluc^{IDS} FRET sensor

To characterize the ability of Fluc^{IDS} to report on changes in conformation via changes in FRET efficiency in real time, single-molecule experiments were performed in which the folded state of Fluc^{IDS} was perturbed with the chemical denaturant GdHCl. To monitor protein unfolding, labeled Fluc^{IDS} incubated in imaging buffer was imaged in the absence of denaturant (i.e., native state) and after 5-min incubation with increasing concentrations of GdHCl (0 to 4 M). The refolding of Fluc^{IDS} denatured in 4 M GdHCl was observed by imaging immediately following the addition of decreasing concentrations of GdHCl (3 to 0 M). To demonstrate the ability of Fluc^{IDS} to report on structural transitions in real time, immobilized Fluc^{IDS} molecules were alternatively incubated in imaging buffer supplemented with or without 4 M GdHCl and the FRET efficiency measured.

Monitoring the refolding of Fluc^{IDS} by the bacterial Hsp70 system

To assess the effect of molecular chaperones on the conformation of a client protein, Fluc^{IDS} was incubated in 4 M GdHCl for 5 min, and the denaturant removed with imaging buffer to generate a misfolded state. To assess the effect of the DnaJ co-chaperone on the conformation of misfolded Fluc^{IDS}, the FRET efficiency of individual molecules were imaged in the presence of increasing concentrations of DnaJ (0 to 10 μM). To assess the effect of DnaK on the conformation of the client, misfolded Fluc^{IDS} was incubated in the presence of DnaJ (0.2 μM) and ATP (5 mM) and increasing concentrations of DnaK (0 to 10 μM). For each condition described above, the imaging buffer containing the indicated concentration of chaperone was injected into the microfluidic channel, data were acquired for 30 min, and the process was repeated with progressively increasing concentrations of chaperone. As a control, the FRET efficiency of Fluc^{IDS} was determined in the presence of DnaK alone (3 μM) or when supplemented with DnaJ (0.2 μM) and the non-hydrolyzable ATP analog, adenylyl-imidodiphosphate (AMP-PNP, 5 mM).

Last, the conformation of Fluc^{IDS} during refolding with the complete KJE system was assessed. To best elucidate the effect of

differing concentrations of GrpE (0 to 6 μM) on the conformation of Fluc^{IDS}, KJE-assisted refolding was performed in the presence of high concentrations of DnaJ (0.6 μM) and DnaK (9 μM) to ensure that binding was efficient (i.e., not limiting for optimal GrpE function) and occurred on ideal time scales at the single-molecule level. Each KJE-assisted refolding reaction was performed in a different microfluidic channel, and smFRET data were acquired for 36 min after addition of the complete KJE system to misfolded Fluc^{IDS}.

To determine whether a single round of chaperone binding and release is sufficient for protein folding, experiments were performed under conditions that promote either binding or release of Fluc^{IDS} by chaperones. A binding cycle was induced upon incubation of Fluc^{IDS} with high concentrations of DnaJ and DnaK (1 and 15 μM , respectively) with ATP (5 mM) to form DnaK-Fluc^{IDS} complexes. A chaperone release cycle was initiated following incubation of the flow cell with a solution containing only GrpE (2 μM) and ATP (5 mM). The binding and release cycles were repeated once.

smFRET analysis

Single-molecule time trajectories were analyzed in MATLAB using the MASH-FRET user interface (version 1.2.2, accessible at <https://rna-fretools.github.io/MASH-FRET/>) (57). The approximate FRET value is measured as the ratio between the acceptor fluorescence intensity (I_{Acceptor}) and the sum of both donor (I_{Donor}) and acceptor fluorescence intensities after correcting for cross-talk between donor and acceptor channels. The formula for calculating the FRET efficiency is given by Eq. 1, whereby the corrected acceptor intensity (denoted as CI_{Acceptor}) is equal to $I_{\text{Acceptor}} - (\gamma \times I_{\text{Donor}})$ and γ is the cross-talk correction constant. γ is calculated as the ratio of fluorescence measured in the acceptor and donor detection channels following direct excitation of a protein labeled with a single donor fluorophore.

$$\text{FRET} = \frac{CI_{\text{Acceptor}}}{CI_{\text{Acceptor}} + I_{\text{Donor}}} \quad (1)$$

Briefly, donor and acceptor fluorescence channels were aligned following a local weighted mean transformation of images of Tetra-Speck fluorescent beads and donor and acceptor fluorescence spots colocalized to identify FRET pairs. Molecules that displayed clear donor and/or acceptor photobleaching events or demonstrated anti-correlated changes in donor and acceptor fluorescence intensity were selected for subsequent analysis. The number of photobleaching events observed was used to determine the number of fluorophores present; only molecules in which a single donor and acceptor photobleaching event was observed were used for further analysis.

Trace processing and HMM fitting

Selected molecules were denoised in MASH-FRET using the NL filter, which has been described previously (58), to accurately identify and quantify transitions between different FRET states during downstream processing. Parameter values were as follows: exponent factor for predictor weight, 5; running average window size, 1; factor for predictor average window sizes, 5. Data were truncated to only include FRET values acquired before donor or acceptor photobleaching. FRET efficiency data were exported to the state finding algorithm vbFRET (version vbFRET_nov12, <https://sourceforge.net/projects/vbFRET/>) and trajectories fit to a HMM to identify discrete FRET states, their residence times, and the transition

distributions between them. Because of the heterogeneous nature of the smFRET trajectories, the fitting algorithm was set to identify a maximum of five FRET states per trajectory as is common for complex datasets (59). Default vbFRET settings were used to fit data to the HMM, with the exception that the mu and beta hyperparameters were changed to 1.5 and 0.5, respectively, to prevent overfitting.

Kinetic analysis of HMM fits

The HMM fits of individual FRET trajectories were further analyzed to extract key kinetic information arising from changes in Fluc^{IDS} conformation. The frequency of FRET transition distributions was plotted as a function of the FRET state before (F_{Before}) and after (F_{After}) each transition as a TDP (fig. S3). To investigate transitions of interest, each transition (as determined from the HMM analysis) was sorted into different directional classes denoted generally as $T_{\text{Before-After}}$, whereby "before" refers to F_{Before} and "after" refers to F_{After} . For simplicity, FRET data were binned according to whether F_{Before} or F_{After} was greater than 0.5 (high) or less than 0.5 (low), unless otherwise indicated, and, thus, four different transition classes are possible: $T_{\text{high-high}}$, $T_{\text{high-low}}$, $T_{\text{low-low}}$, and $T_{\text{low-high}}$. To determine the relative occurrence of transitions of interest, the number of transitions for each transition class was normalized to the total number of transitions measured from all classes. The residence time (defined as the time that a molecule resides at F_{Before} before transition to F_{After}) for each transition within a transition class was calculated and presented as the means \pm SEM (fig. S3). Last, the rate of chaperone binding and release events was determined by calculating the number of transitions to FRET states below (i.e., binding event) or above (i.e., release event) the FRET threshold set for DnaK binding (0.2 FRET) for each molecule. From here, the minimum number of binding or release events was divided by the imaging lifetime of that molecule (i.e., time until photobleaching) to determine the binding and release rate. Because it is not possible to determine for how long a particular FRET state would have existed if not truncated because of photobleaching, the last measured residence times were deleted from the dataset to extract true residence times. Because data were smoothed during denoising, residence times shorter than that given by Eq. 2 were not considered for further analysis. F is the imaging frame rate in milliseconds, and N_{FA} is the number of frames that were averaged during trace denoising.

$$\text{Residence time}_{\text{Delete}} = 2 \cdot F \cdot N_{\text{FA}} \quad (2)$$

To determine how molecular chaperones affect the lifetime of certain FRET states, the residence times for each transition class were statistically analyzed using a one-way or two-way analysis of variance (ANOVA) with either a Šidák or Tukey's multiple-comparisons post hoc test, with $P \leq 0.05$ determined to be statistically significant.

Histogram and population analysis

The FRET efficiency of all data points for each molecule was collated and presented as FRET efficiency histograms. To identify the proportion of the different Fluc^{IDS} states within the smFRET data (e.g., Hsp70-bound, native, or misfolded), histograms were fit to a mixed Gaussian model. Native Fluc^{IDS} was fit to a normally distributed Gaussian. Because of the non-linear relationship between dye-pair distances and the FRET efficiency, FRET populations with theoretical dye-pair distances that are significantly deviated from the

Förster radius (5.1 nm for AF555/AF647), such as Hsp70-bound and misfolded Fluc^{IDS} populations, need to be fit to skewed Gaussian models (fig. S10). Native or misfolded states of Fluc^{IDS} were fit to their respective Gaussian shapes without parameter constraints in the absence of chaperones, and the sigma, center, and gamma (for the skewed Gaussian model) parameter values were used as a guide when analyzing smFRET data acquired in the presence of chaperones. The area under each curve was determined and normalized to the combined area of all Gaussians curves to determine the proportion of each Fluc^{IDS} state.

Statistical analysis

All data analysis and presentation were performed using custom-written scripts on Python software or using GraphPad Prism 9 (GraphPad Software Inc., San Diego, USA).

Supplementary Materials

This PDF file includes:

Figs. S1 to S10

[View/request a protocol for this paper from Bio-protocol.](#)

REFERENCES AND NOTES

- C. M. Dobson, Protein folding and misfolding. *Nature* **426**, 884–890 (2003).
- D. Fraser-Pitt, D. O'Neil, Cystic fibrosis - A multiorgan protein misfolding disease. *Futur. Sci.* **1**, FSO57 (2015).
- W. Dauer, S. Przedborski, Parkinson's disease. *Neuron* **39**, 889–909 (2003).
- R. J. W. Truscott, Age-related nuclear cataract-oxidation is the key. *Exp. Eye Res.* **80**, 709–725 (2005).
- D. R. Thal, M. Fändrich, Protein aggregation in Alzheimer's disease: A β and τ and their potential roles in the pathogenesis of AD. *Acta Neuropathol.* **129**, 163–165 (2015).
- F. U. Hartl, A. Bracher, M. Hayer-Hartl, Molecular chaperones in protein folding and proteostasis. *Nature* **475**, 324–332 (2011).
- R. P. Taylor, I. J. Benjamin, Small heat shock proteins: A new classification scheme in mammals. *J. Mol. Cell. Cardiol.* **38**, 433–444 (2005).
- F. Chiti, C. M. Dobson, Protein misfolding, amyloid formation, and human disease: A summary of progress over the last decade. *Annu. Rev. Biochem.* **86**, 27–68 (2017).
- G. Calloni, T. Chen, S. M. Schermann, H. Chang, P. Genevoux, F. Agostini, G. G. Tartaglia, M. Hayer-Hartl, F. U. Hartl, DnaK functions as a central hub in the E. coli chaperone network. *Cell Rep.* **1**, 251–264 (2012).
- P. Goloubinoff, Editorial: The HSP70 molecular chaperone machines. *Front. Mol. Biosci.* **4**, 1–4 (2017).
- J. Bonomo, J. P. Welsh, K. Manthiram, J. R. Swartz, Comparing the functional properties of the Hsp70 chaperones, DnaK and BiP. *Biophys. Chem.* **149**, 58–66 (2010).
- S. Wisén, J. E. Gestwicki, Identification of small molecules that modify the protein folding activity of heat shock protein 70. *Anal. Biochem.* **374**, 371–377 (2008).
- T. M. Luengo, R. Kityk, M. P. Mayer, S. G. D. Rüdiger, Hsp90 breaks the deadlock of the Hsp70 chaperone system. *Mol. Cell* **70**, 545–552.e9 (2018).
- A. Szabo, T. Langer, H. Schroder, J. Flanagan, B. Bukau, F. U. Hartl, The ATP hydrolysis-dependent reaction cycle of the *Escherichia coli* Hsp70 system DnaK, DnaJ, and GrpE. *Proc. Natl. Acad. Sci. U.S.A.* **91**, 10345–10349 (1994).
- T. Laufen, M. P. Mayer, C. Beisel, D. Klostermeier, A. Mogk, J. Reinstein, B. Bukau, Mechanism of regulation of Hsp70 chaperones by DnaJ cochaperones. *Proc. Natl. Acad. Sci. U.S.A.* **96**, 5452–5457 (1999).
- R. Russell, A. Wali Karzai, A. F. Mehl, R. McMacken, DnaJ dramatically stimulates ATP hydrolysis by DnaK: Insight into targeting of Hsp70 proteins to polypeptide substrates. *Biochemistry* **38**, 4165–4176 (1999).
- A. Sekhar, A. Velyvis, G. Zoltsman, R. Rosenzweig, G. Bouvignies, L. E. Kay, Conserved conformational selection mechanism of Hsp70 chaperone-substrate interactions. *eLife* **7**, e32764 (2018).
- R. Kellner, H. Hofmann, A. Barducci, B. Wunderlich, D. Nettels, B. Schuler, Single-molecule spectroscopy reveals chaperone-mediated expansion of substrate protein. *Proc. Natl. Acad. Sci. U.S.A.* **111**, 13355–13360 (2014).
- R. Imamoglu, D. Balchin, M. Hayer-Hartl, F. U. Hartl, Bacterial Hsp70 resolves misfolded states and accelerates productive folding of a I protein. *Nat. Commun.* **11**, 365 (2020).
- V. Dahiya, G. Agam, J. Lawatscheck, D. A. Rutz, D. C. Lamb, J. Buchner, Coordinated conformational processing of the tumor suppressor protein p53 by the Hsp70 and Hsp90 chaperone machineries. *Mol. Cell* **74**, 816–830.e7 (2019).
- S. K. Sharma, P. De los Rios, P. Christen, A. Lustig, P. Goloubinoff, The kinetic parameters and energy cost of the Hsp70 chaperone as a polypeptide unfoldase. *Nat. Chem. Biol.* **6**, 914–920 (2010).
- K. Tsuboyama, H. Tadakuma, Y. Tomari, Conformational activation of argonaute by distinct yet coordinated actions of the Hsp70 and Hsp90 chaperone systems. *Mol. Cell* **70**, 722–729.e4 (2018).
- E. J. Levy, J. McCarty, B. Bukau, W. J. Chirico, Conserved ATPase and luciferase refolding activities between bacteria and yeast Hsp70 chaperones and modulators. *FEBS Lett.* **368**, 435–440 (1995).
- N. B. Nillegoda, J. Kirstein, A. Szlachcik, M. Berynskyy, A. Stank, F. Stengel, K. Arnsburg, X. Gao, A. Scior, R. Aebbersold, D. L. Guilbride, R. C. Wade, R. I. Morimoto, M. P. Mayer, B. Bukau, Crucial HSP70 co-chaperone complex unlocks metazoan protein disaggregation. *Nature* **524**, 247–251 (2015).
- N. Hristozova, P. Tompa, D. Kovacs, A novel method for assessing the chaperone activity of proteins. *PLOS ONE* **11**, e0161970 (2016).
- T. Rosenkranz, R. Schlesinger, M. Gabba, J. Fitter, Native and unfolded states of phosphoglycerate kinase studied by single-molecule FRET. *ChemPhysChem* **12**, 704–710 (2011).
- B. Schuler, E. A. Lipman, W. A. Eaton, Probing the free-energy surface for protein folding with single-molecule fluorescence spectroscopy. *Nature* **419**, 743–747 (2002).
- E. V. Kuzmenkina, C. D. Heyes, G. U. Nienhaus, Single-molecule Förster resonance energy transfer study of protein dynamics under denaturing conditions. *Proc. Natl. Acad. Sci. U.S.A.* **102**, 15471–15476 (2005).
- T. Tezuka-Kawakami, C. Gell, D. J. Brockwell, S. E. Radford, D. A. Smith, Urea-induced unfolding of the immunity protein Im9 monitored by spFRET. *Biophys. J.* **91**, L42–L44 (2006).
- A. Mashaghi, S. Mashaghi, S. J. Tans, Misfolding of luciferase at the single-molecule level. *Angew. Chemie* **53**, 10390–10393 (2014).
- Z. N. Scholl, W. Yang, P. E. Marszalek, Chaperones rescue luciferase folding by separating its domains. *J. Biol. Chem.* **289**, 28607–28618 (2014).
- F. Rodriguez, F. Arsène-Ploetze, W. Rist, S. Rüdiger, J. Schneider-Mergener, M. P. Mayer, B. Bukau, Molecular basis for regulation of the heat shock transcription factor σ 32 by the DnaK and DnaJ chaperones. *Mol. Cell* **32**, 347–358 (2008).
- Y. Jiang, P. Rossi, C. G. Kalodimos, Structural basis for client recognition and activity of Hsp40 chaperones. *Science* **365**, 1313–1319 (2019).
- M. P. Mayer, Hsp70 chaperone dynamics and molecular mechanism. *Trends Biochem. Sci.* **38**, 507–514 (2013).
- E. M. Clerico, J. M. Tilitsky, W. Meng, L. M. Gierasch, How Hsp70 molecular machines interact with their substrates to mediate diverse physiological functions. *J. Mol. Biol.* **427**, 1575–1588 (2015).
- P. Goloubinoff, P. D. L. Rios, The mechanism of Hsp70 chaperones: (Entropic) pulling the models together. *Trends Biochem. Sci.* **32**, 372–380 (2007).
- S. Rüdiger, J. Schneider-Mergener, B. Bukau, Its substrate specificity characterizes the DnaJ co-chaperone as a scanning factor for the DnaK chaperone. *EMBO J.* **20**, 1042–1050 (2001).
- K. Terada, Y. Oike, Multiple molecules of Hsc70 and a dimer of DjA1 independently bind to an unfolded protein. *Appl. Microbiol. Biotechnol.* **285**, 16789–16797 (2010).
- J. Perales-Calvo, A. Muga, F. Moro, Role of DnaJ G/F-rich domain in conformational recognition and binding of protein substrates. *J. Biol. Chem.* **285**, 34231–34239 (2010).
- T. Langer, C. Lu, H. Echols, J. Flanagan, M. K. Hayer, F. U. Hartl, Successive action of DnaK, DnaJ and GroEL along the pathway of chaperone-mediated protein folding. *Nature* **356**, 683–689 (1992).
- L. Packschies, H. Theyssen, A. Buchberger, B. Bukau, A. Roger, S. Goody, J. Reinstein, GrpE accelerates nucleotide exchange of the molecular chaperone DnaK with an associative displacement mechanism. *Biochemistry* **36**, 3417–3422 (1997).
- D. Brehmer, S. Rüdiger, C. S. Gässler, D. Klostermeier, L. Packschies, J. Reinstein, M. P. Mayer, B. Bukau, Tuning of chaperone activity of Hsp70 proteins by modulation of nucleotide exchange. *Nat. Struct. Biol.* **8**, 427–432 (2001).
- H. Saibil, Chaperone machines for protein folding, unfolding and disaggregation. *Nat. Rev. Mol. Cell Biol.* **14**, 630–642 (2013).
- R. Rosenzweig, N. B. Nillegoda, M. P. Mayer, B. Bukau, The Hsp70 chaperone network. *Nat. Rev. Mol. Cell Biol.* **20**, 665–680 (2019).
- D. Balchin, M. Hayer-Hartl, F. U. Hartl, Recent advances in understanding catalysis of protein folding by molecular chaperones. *FEBS Lett.* **594**, 2770–2781 (2020).
- P. Koldewey, S. Horowitz, J. C. A. Bardwell, Chaperone-client interactions: Non-specificity engenders multifunctionality. *J. Biol. Chem.* **292**, 12010–12017 (2017).

47. P. De Los Rios, A. Barducci, Hsp70 chaperones are non-equilibrium machines that achieve ultra-affinity by energy consumption. *eLife* **3**, e02218 (2014).
48. S. Assenza, A. S. Sassi, R. Kellner, B. Schuler, P. De Los Rios, A. Barducci, Efficient conversion of chemical energy into mechanical work by Hsp70 chaperones. *eLife* **8**, e48491 (2019).
49. S. Tiwari, B. Fauvet, S. Assenza, P. D. los Rios, P. Goloubinoff, A novel fluorescent multi-domain protein construct reveals the individual steps of the unfoldase action of Hsp70. *bioRxiv* 2022.02.17.480908 [Preprint]. 17 February 2022. <https://doi.org/10.1101/2022.02.17.480908>.
50. A. Sekhar, R. Rosenzweig, G. Bouvignies, L. E. Kay, Mapping the conformation of a client protein through the Hsp70 functional cycle. *Proc. Natl. Acad. Sci. U.S.A.* **112**, 10395–10400 (2015).
51. J. H. Lee, D. Zhang, C. Hughes, Y. Okuno, A. Sekhar, S. Cavagnero, Heterogeneous binding of the SH3 client protein to the DnaK molecular chaperone. *Proc. Natl. Acad. Sci. U.S.A.* **112**, E4206–E4215 (2015).
52. J. Lu, X. Zhang, Y. Wu, Y. Sheng, W. Li, W. Wang, Energy landscape remodeling mechanism of Hsp70-chaperone-accelerated protein folding. *Biophys. J.* **120**, 1971–1983 (2021).
53. R. Rosenzweig, A. Sekhar, J. Nagesh, L. E. Kay, Promiscuous binding by Hsp70 results in conformational heterogeneity and fuzzy chaperone-substrate ensembles. *eLife* **6**, e28030 (2017).
54. Y. Kim, S. O. Ho, N. R. Gassman, Y. Korlann, E. V. Landorf, F. R. Collart, S. Weiss, Efficient site-specific labeling of proteins via cysteines. *Bioconjug. Chem.* **19**, 786–791 (2008).
55. S. D. Chandradoss, A. C. Haagsma, Y. K. Lee, J.-H. Hwang, J.-M. Nam, C. Joo, Surface passivation for single-molecule protein studies. *J. Vis. Exp.* **86**, 1–8 (2014).
56. H. Pan, Y. Xia, M. Qin, Y. Cao, W. Wang, A simple procedure to improve the surface passivation for single molecule fluorescence studies. *Phys. Biol.* **12**, 045006 (2015).
57. M. C. A. S. Hadzic, R. Börner, S. L. B. König, D. Kowanko, R. K. O. Sigel, Reliable state identification and state transition detection in fluorescence intensity-based single-molecule Förster resonance energy-transfer data. *J. Phys. Chem. B* **122**, 6134–6147 (2018).
58. G. Haran, Noise reduction in single-molecule fluorescence trajectories of folding proteins. *Chem. Phys.* **307**, 137–145 (2004).
59. M. Blanco, N. G. Walter, Analysis of complex single-molecule FRET time trajectories. *Methods Enzymol.* **472**, 153–178 (2010).
60. E. Conti, N. P. Franks, P. Brick, Crystal structure of firefly luciferase throws light on a superfamily of adenylate-forming enzymes. *Structure* **4**, 287–298 (1996).

Acknowledgments: We would like to thank T. Böcking for designing and providing the initial Fluc^{IDS} smFRET construct. We would also like to thank M. Mayer for providing expression plasmids for the bacterial chaperones KJE. We would also like to acknowledge D. Cox (University of Cambridge, UK) for useful advice when writing the smFRET analysis code. Last, we thank the staff in Molecular Horizons and the Illawarra Health and Medical Research Institute for technical and administrative support. **Funding:** A.M.v.O. and H.E. acknowledge funding from the Australian Research Council (DP220103466). A.M.v.O. also acknowledges funding from the National Health and Medical Research Council (APP1197069). **Author contributions:** N.R.M., B.P.P., H.E., and A.M.v.O. formulated the experimental approach. N.R.M. performed all experiments, curated and analyzed data, constructed figures, and wrote the initial manuscript. N.R.M., B.P.P., H.E., and A.M.v.O. edited the manuscript and approved submission of the final manuscript. **Competing interests:** The authors declare that they have no competing interests. **Data and materials availability:** All data needed to evaluate the conclusions in the paper are present in the paper and/or the Supplementary Materials. All unique reagents generated in this study are available from the lead contact without restriction. Single-molecule and other raw data materials needed to evaluate the conclusions in the paper has been deposited at Zenodo at the following DOI:10.5281/zenodo.7069666. All original code has been deposited at Zenodo at the following DOI:10.5281/zenodo.6392452. Further information and requests for resources and reagents should be directed to and will be fulfilled by the lead contacts, H.E. (heathe@uow.edu.au) and A.M.v.O. (vanoijen@uow.edu.au).

Submitted 23 May 2022
Accepted 10 November 2022
Published 14 December 2022
10.1126/sciadv.add0922